Received: 15 April 2024 | Revised: 28 May 2024 | Accepted: 30 May 2024

DOI: 10.1002/pro.5078

RESEARCH ARTICLE

THE PROTEIN SOCIETY WILEY

Tubulin-binding region alters tau–lipid interactions and changes toxicity of tau fibrils formed in the presence of phosphatidylserine lipids

Abid Ali[1] | **Aidan P. Holman**[1,2] | **Axell Rodriguez**[1] | **Mikhail Matveyenka**[1] | **Dmitry Kurouski**[1,3]

[1]Department of Biochemistry and Biophysics, Texas A&M University, College Station, Texas, USA

[2]Department of Entomology, Texas A&M University, College Station, Texas, USA

[3]Department of Biomedical Engineering, Texas A&M University, College Station, Texas, USA

Correspondence
Dmitry Kurouski, Department of Biomedical Engineering, Texas A&M University, College Station, Texas, 77843, USA.
Email: dkurouski@tamu.edu

Funding information
National Institute of General Medical Sciences, Grant/Award Number: R35GM142869

Review Editor: Aitziber L. Cortajarena

Abstract

Alzheimer's disease is the fastest-growing neurodegenerative disease that affects over six million Americans. The abnormal aggregation of amyloid β peptide and Tau protein is the expected molecular cause of the loss of neurons in brains of AD patients. A growing body of evidence indicates that lipids can alter the aggregation rate of amyloid β peptide and modify the toxicity of amyloid β aggregates. However, the role of lipids in Tau aggregation remains unclear. In this study, we utilized a set of biophysical methods to determine the extent to which phospatidylserine (PS) altered the aggregation properties of Tau isoforms with one (1N4R) and two (2N4R) N terminal inserts that enhance the binding of Tau to tubulin. We found that the length and saturation of fatty acids (FAs) in PS altered the aggregation rate of 2N4R isoform, while no changes in the aggregation rate of 1N4R were observed. These results indicate that N terminal inserts play an important role in protein–lipid interactions. We also found that PS could change the toxicity of 1N4R and 2N4R Tau fibrils, as well as alter molecular mechanisms by which these aggregates exert cytotoxicity to neurons. Finally, we found that although Tau fibrils formed in the presence and absence of PS endocytosed by cells, only fibril species that were formed in the presence of PS exert strong impairment of the cell mitochondria.

KEYWORDS

1N4R tau, 2N4R tau, AFM-IR, fibrils, oligomers, phosphatidylserine, toxicity

1 | INTRODUCTION

Tau proteins play the central role in assembly and stabilization of microtubules in neurons (Gouras et al., 2010; McLean et al., 1999). The isoforms are produced as a result of alternative splicing of exons 2, 3, and 10 (Goedert et al., 1989; Himmler et al., 1989). Full-length $Tau_{1\text{-}441}$ contains two N terminal inserts (2N4R) that enhance the binding of Tau to tubulin (Grundke-Iqbal et al., 1986; Weingarten et al., 1975). In addition to the full-length Tau, its isoform with one N terminal insert (1N4R) is involved in microtubules' stabilization (Alonso Adel et al., 2004; Alonso et al., 2001).

In the presence of promoters such as heparin, Tau isoforms can aggregate forming amyloid oligomers and fibrils (Falcon et al., 2019; Giamblanco et al., 2020; Zhang et al., 2019). These protein aggregates are found in neurofibrillary tangles (NFTs), intracellular formations that are

commonly observed in patients diagnosed with Alzheimer's disease (AD) (Ait-Bouziad et al., 2017; Takashima, 2013). Tau oligomers and fibrils exhibit high morphological heterogeneity and cytotoxicity (Eisenberg & Sawaya, 2017; Karikari et al., 2019; Lasagna-Reeves, Castillo-Carranza, Sengupta, Sarmiento, et al., 2012; Shafiei et al., 2017; Takashima, 2013). Furthermore, injection of Tau oligomers into the brain of wide-type mice caused cognitive, synaptic, and mitochondrial abnormalities that were not observed upon Tau monomer injections (Lasagna-Reeves, Castillo-Carranza, Jackson, & Kayed, 2011; Lasagna-Reeves, Castillo-Carranza, Sengupta, et al., 2011). Tau oligomers also induce endogenous Tau to misfold and propagate from affected to unaffected brain regions in mice, whereas fibrils do not exhibit such seeding behavior (Lasagna-Reeves, Castillo-Carranza, Sengupta, Guerrero-Munoz, et al., 2012). The pathological progression of AD has been attributed to the prion-like self-propagation of Tau aggregates following the route of anatomically connected neurons (Nath et al., 2012; Rajendran et al., 2006; Wang et al., 2017). The cell-to-cell transfer of Tau aggregates has been demonstrated in in vitro neuronal models (Clavaguera et al., 2009; Nath et al., 2012). Specifically, Tau oligomers exhibited fast axonal transport in the anterograde direction at all physiological Tau levels (LaPointe et al., 2009; Morfini et al., 2009).

Ait-Bouziad and co-workers found that 2N4R and its K18 isoform strongly interacted with phosphatidylserine (PS), anionic lipid that is primarily localized on the inner part of plasma membranes (Ait-Bouziad et al., 2017). As a result of such interactions, highly toxic Tau-PS oligomers were formed (Ait-Bouziad et al., 2017). Using NMR, the researchers found that protein and lipids in the oligomers were held together by strong electrostatic interactions between the charged amino acids residues of Tau and polar heads of PS (Ait-Bouziad et al., 2017). Yao and co-workers found that not only the presence of PS, but also protein-to-lipid ratio strongly influenced the conformation of Tau (Yao et al., 2022).

Recently reported results by our group showed that stability of amyloidogenic proteins, as well as toxicity of their oligomers and fibrils could be altered by the length and saturation of fatty acids (FAs) in phospholipids (Ali et al., 2023a; Dou et al., 2021; Dou et al., 2023; Dou & Kurouski, 2022). Specifically, α-synuclein (α-syn), a protein that is strongly connected to Parkinsons's disease, formed more toxic fibrils in the presence of 1-palmitoyl-2-oleoyl-sn-glycero-3-phosphoL-serine (POPS) than in the lipid-free environment (Ali et al., 2023b). At the same time, 1,2-dioleoyl-sn-glycero-3-phosphoL-serine (DOPS) and 1,2-distearyl-sn-glycero-3-phospho-Lserine (DSPS) drastically reduced the toxicity of α-syn if were present during protein aggregation (Ali et al., 2023b). However, the role of the length and saturation of FAs in PS on the aggregation properties of two Tau isoforms remains unclear.

In this study, we utilized a set of biophysical techniques to determine the extent to which 1,2-dimyristoyl-*sn*-glycero-3-phosphoLserine (DMPS), POPS, DOPS, and DSPS altered the aggregation rate of 1N4R and 2N4R Tau, Scheme 1. It should be noted that PS plays a critical role in recognition of malfunctional cells by macrophages (Levental et al., 2020; Matveyenka et al., 2022). In healthy cells, PS is localized on the cytosolic side of plasma membrane via ATP-dependent transport (Alecu & Bennett, 2019; Fitzner et al., 2020). In pre- and apoptotic cells, PS is translocated to the exterior part of the membrane (Levental et al., 2020; Matveyenka et al., 2022). If such malfunctioning cells are not eliminated by macrophages, PS domains in the plasma membrane can trigger the aggregation of misfolded proteins present close to the membrane surface (Ali et al., 2023b; Matveyenka, Zhaliazka, & Kurouski, 2023). Thus, one can expect that deceleration of the efficiency of clearance of pre- and apoptotic cells by macrophages can be the underlying cause of the abrupt protein aggregation of Tau proteins.

We also analyzed morphology and secondary structure of Tau fibrils formed in the presence of these phospholipids. Finally, using N27 rat dopaminergic cells, we examined the extent to which PS with different length and saturation of FAs changed the toxicity of 1N4R and 2N4R fibrils.

2 | RESULTS

Kinetic studies of 2N4R and 1N4R Tau aggregation in the presence of POPS, DOPS, DMPS and DSPS.

We utilized ThT assay to examine the extent to which the presence of PSs with different length and saturation of FAs altered the aggregation kinetics of 2N4R and 1N4R Tau. In the lipid-free environment, 2N4R Tau aggregated exhibited a well-defined lag-phase ($t_{lag} = 20.34\ h \pm 2.49\ h$) that was followed by a rapid increase in ThT fluorescence, Figures 1, S1 and S2. Such an increase in ThT fluorescence indicates the formation of amyloid fibrils. We found that the presence of both POPS and DOPS significantly delayed t_{lag} of 2N4R Tau aggregation ($t_{lag} = 48.23\ h \pm 4.49\ h$ and $t_{lag} = 49.34\ h \pm 1.90\ h$, respectively). Substantially smaller changes in t_{lag} were exerted by DMPS ($t_{lag} = 29.01\ h \pm 1.63\ h$). Finally, we found that DSPS did not alter t_{lag} if was present at 1:1 molar ratio with 2N4R Tau. Thus, we can conclude that both saturation and length of FAs in PS play an important role in the self-assembly of 2N4R Tau. PS

SCHEME 1 The amino acid sequence of 2N4R Tau (top) with basic amino acids shown in blue, polar in green, acidic in red and nonpolar in brown. The N2 region missing in 1N4R is shown with a red frame. Molecular structures (bottom) of POPS, DOPS, DMPS and DSPS.

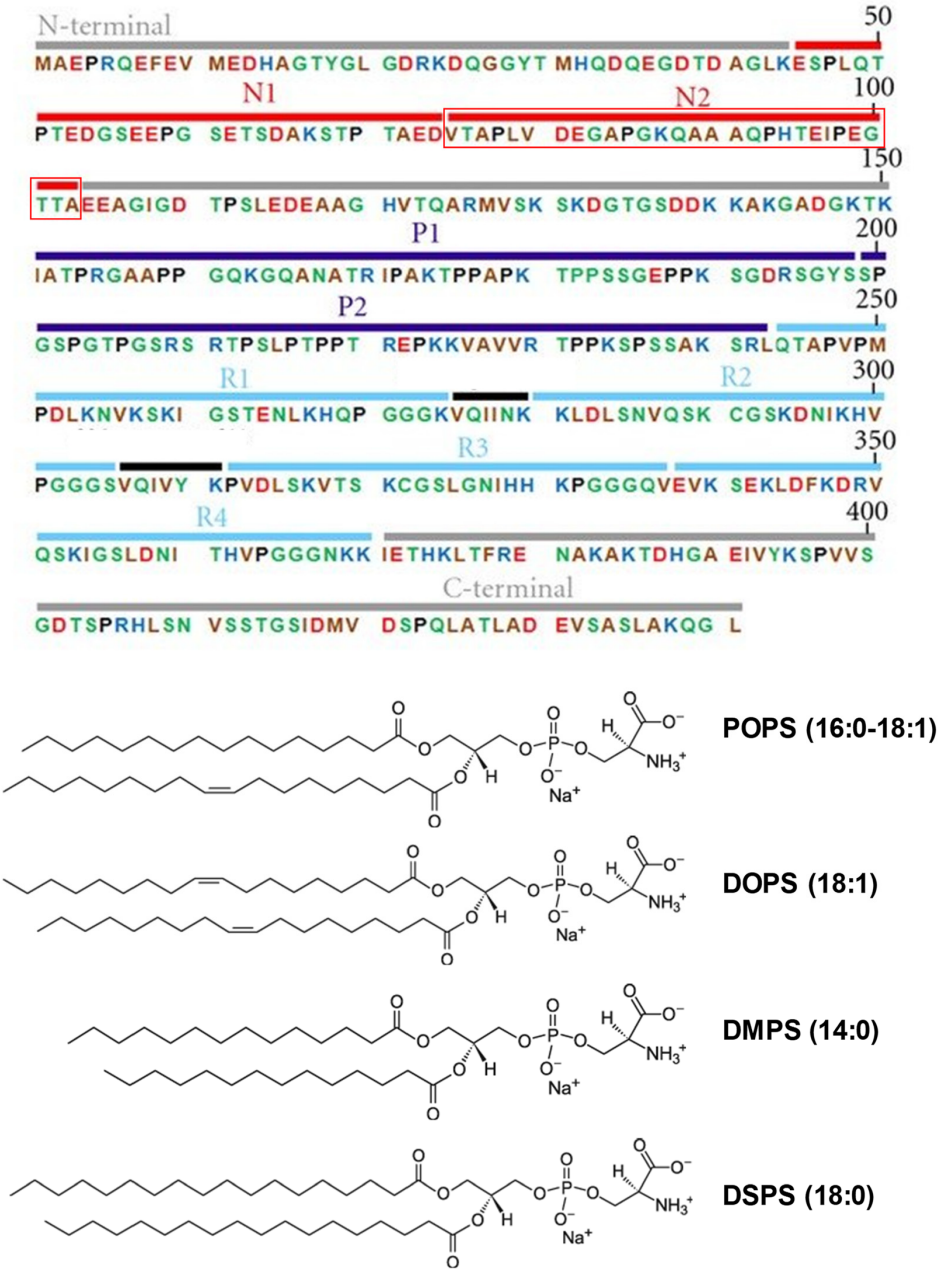

with unsaturated FAs strongly delayed primary nucleation of 2N4R Tau, whereas this effect was less prominent for PS with saturated FAs. Finally, no effect was observed for C18:0 FAs present in DSPS, whereas C14:0 FAs of DMPS only slightly delayed t_{lag} of 2N4R Tau aggregation.

Our kinetic studies also showed that the length and saturation of FAs in PS were less critical for the growth of 2N4R oligomers into fibrils. This conclusion could be made by the analysis of half-time ($t_{1/2}$) of protein aggregation kinetics. It should be noted that fragmentation and secondary nucleation take place in parallel with fibril elongation. Therefore, $t_{1/2}$ can be only tentatively used to understand the rate of fibril growth. Specifically, we found that $t_{1/2}$ of 2N4R Tau did not much change in the presence of POPS, DOPS, and DSPS ($t_{1/2} = 69.79$ h $\pm$ 5.2 h, $t_{1/2} = 73.90$ h $\pm$ 8.433 h and $t_{1/2} = 62.12$ h $\pm$ 1.93 h, respectively). We only observed a small increase in the growth rate of 2N4R Tau in the presence of DMPS $t_{1/2} = 51.01$ h $\pm$ 3.81 h, Figure 1. Based on these results, we can conclude that DOPS, POPS, and DSPS do not alter the growth rate of 2N4R fibrils.

ThT kinetics revealed completely different relationships between 1N4R Tau and PS with different length and saturation of FAs. Specifically, we found that none of PSs changed t_{lag} duration of 1N4R Tau, Figure 1. These findings demonstrate that the length and saturation of FAs in PS have no effect on the primary

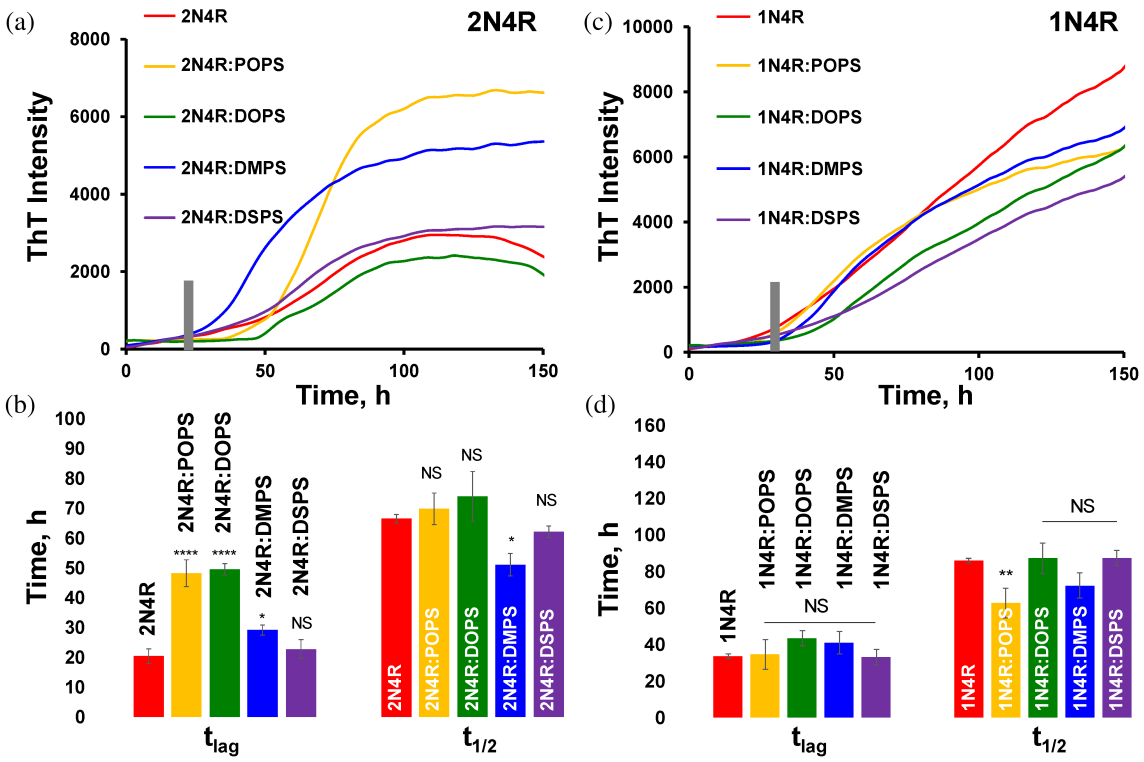

FIGURE 1 Kinetics of protein aggregation. ThT kinetics (a and c) together with corresponding histograms of t_{lag} and $t_{1/2}$ (b and d) of 2N4R and 1N4R aggregation in lipid-free environment (red), as well as in the presence of POPS (yellow), DOPS (green), DMPS (blue) and DSPS (purple). Gray vertical lines indicate t_{lag} of 2N4R and 1N4R Tau aggregation. According to one-way ANOVA, $^{*}p < 0.05$, $^{**}p < 0.01$, $^{***}p < 0.001$, $^{****}p < 0.0001$. NS shows the absence of statistically significant differences.

nucleation of 1N4R Tau. Similar conclusion could be made about the rate of 1N4R fibril formation except for POPS ($t_{lag} = 34.45$ h $\pm$ 8.16 h) that was found to accelerate the elongation of 1N4R Tau oligomers into fibrils. Based on these results, we can conclude that N2 region of Tau plays a critically important role in protein–lipid interactions. Furthermore, this region allows aliphatic tails of PS to alter the rate of protein aggregation. Previously used NMR revealed that α-syn–lipid interactions were primarily based on electrostatic and hydrophobic interactions (Bodner et al., 2009; Bodner et al., 2010; Maltsev et al., 2013; Ysselstein et al., 2015). Although there no such studies for Tau, our results suggest that Tau–PS interactions are primarily based on electrostatic and hydrophobic interactions, one can expect that polar, charged and non-polar amino acids of N2 region play a key role in the interactions that take place between Tau and lipids. It should be noted that N2 region of Tau plays an important role in the protein aggregation in the lipid-free environment. Specifically, ThT curves of 2N4R Tau exhibit an exponential increase followed by a plateau, while the 1N4R Tau curves show a linear increase. These results suggest that 2 N retain may alter oligomer formation and, consequently, nucleation of Tau aggregation.

Morphological characterization of 2N4R and 1N4R Tau aggregates grown in the presence of POPS, DOPS, DMPS and DSPS, as well as in the lipid-free environment.

We utilized atomic force microscopy (AFM) to examine the morphology of protein aggregates formed in the presence of PS with different length and saturation of FAs. We found that in the lipid-free environment, 2N4R Tau formed thin fibrils that had ~ 7–8 nm in height, Figure 2. Substantially thinner fibrils were observed in 2N4R:POPS, 2N4R:DOPS, 2N4R:DMPS, and 2N4R:DSPS. Specifically, most of 2N4R:DOPS fibrils were only 2–4 nm in height, whereas the height of 2N4R:POPS and 2N4R:DMPS ranged within 4–6 nm. These results indicate that POPS and DMPS may facilirate laternal assembly or intertwining of thinner (2–4 nm) fibrils into such thick bundles. 2N4R:DSPS fibrils had a larger distribution of heights ranging from 4 to 8 nm, Figure 2. These fibrils were much wider than other amyloid aggregates. Finally, we found that length of 2N4R:DMPS fibrils was the shortest compared to all other samples. Thus, we can conclude that the length and saturation of FAs in PS uniquely altered the morphology of 2N4R fibrils. Specifically, in the presence of PS with unsaturated FAs (POPS and DOPS), 2N4R Tau formed thinner fibrils compared to

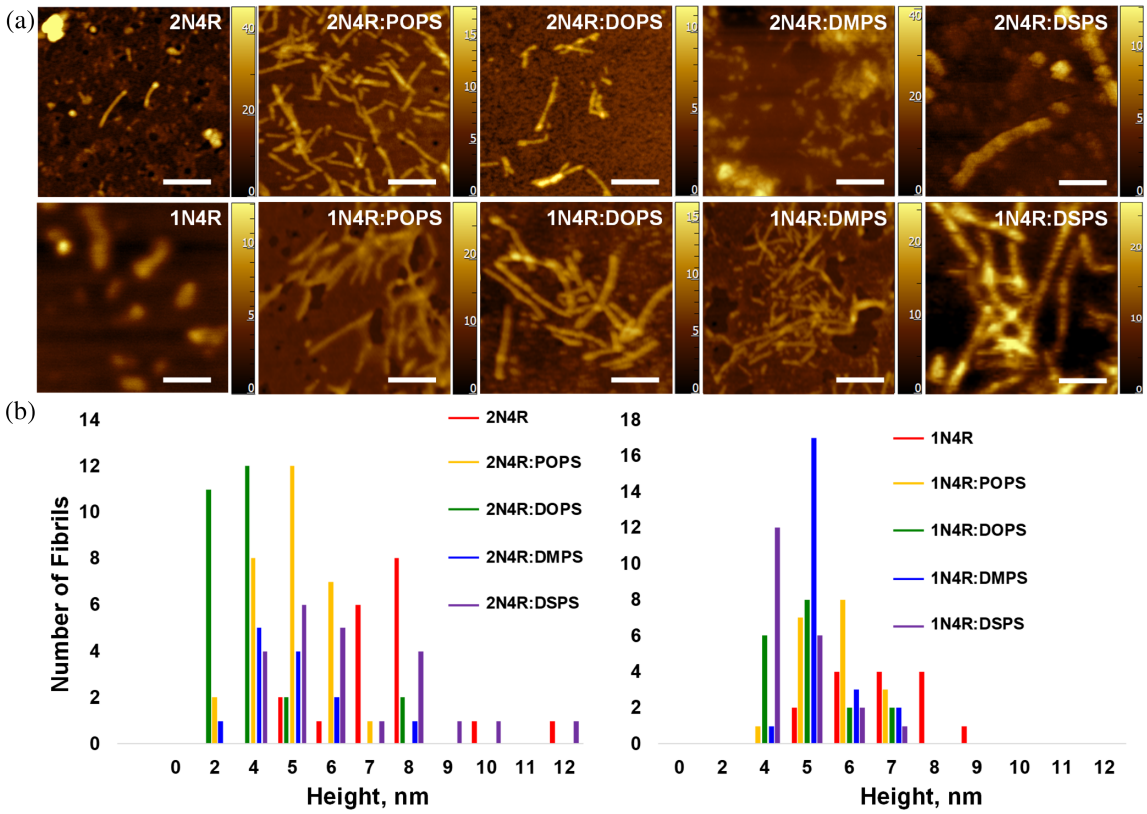

FIGURE 2 Morphology of protein aggregates. AFM images (a) together with the corresponding height histograms (b) of 2N4R and 1N4R aggregates formed in lipid-free environment (red), as well as in the presence of POPS (yellow), DOPS (green), DMPS (blue) and DSPS (purple).

2N4R Tau fibrils formed in the lipid-free environment. In the presence of C14:0 FAs (DMPS), 2N4R formed very short and thin fibrils, whereas in the presence of C18:0 FAs, thin but wide 2N4R Tau fibrils were observed.

In the lipid-free environment, 1N4R formed similar fibrillar species with heights ranging from 5 to 9 nm, Figure 2. We found that fibrils with similar height profiles were observed in 1N4R:POPS, 1N4R:DOPS, 1N2R:DMPS, and 1N2R:DSPS. However, their heights were smaller (4–7 nm). Based on these results, we can conclude that PS makes 1N4R Tau form fibrils with slightly lower heights. Morphologies of 1N4R:POPS fibrils were highly similar to the protein aggregates observed in 1N4R:DOPS and 1N2R:DMPS. However, much longer fibrils were observed in 1N4R:DSPS. Thus, we can conclude that the height of 1N4R fibrils can be altered by the length and saturation of FAs in PS.

Structural characterization of 2N4R and 1N4R Tau aggregates grown in the presence of POPS, DOPS, DMPS and DSPS, as well as in the lipid-free environment.

We utilized circular dichroism (CD) and nano-Infrared spectroscopy (nano-IR) to examine the secondary structure of protein aggregates formed in the presence of PS with different length and saturation of FAs, Figure 3. CD spectra acquired from 2N4R fibrils grown in the presence of POPS, DOPS, DMPS and DSPS, as well as in the lipid-free environment exhibited a minimum at ~218 nm, Figure 3, A. This indicates the predominance of β-sheet in their secondary structure. Similar CD spectra were observed for 1N4R fibrils. However, we observed a small shift of their minima to 220 nm, which indicates small changes in the secondary structure of 1N4R fibrils compared to the secondary structure of 2N4R aggregates, Figure 3b.

In nano-IR, also known as atomic force microscopy Infrared (AFM-IR) spectroscopy, a metallized scanning probe can be positioned directly at the specimen of interest. Next, pulsed tunable IR light is used to induce thermal expansions in the sample, which are recorded by the probe and converted into IR spectra. Thus, nano-IR can be used to probe the secondary structure of single protein molecules, as well as individual oligomers and fibrils. In the acquired nano-IR spectra, we observed both amide I (1620–1700 cm^{-1}), amide II (1500–1580 cm^{-1}) and Cα-H (~1460 cm^{-1}) bands, Figure 3c. Quantitative analysis of amide I band revealed that 2N4R Tau fibrils had predominately parallel β-sheet (~50%), with a smaller amount of anti-parallel β-sheet (~25%), α-helix and unordered

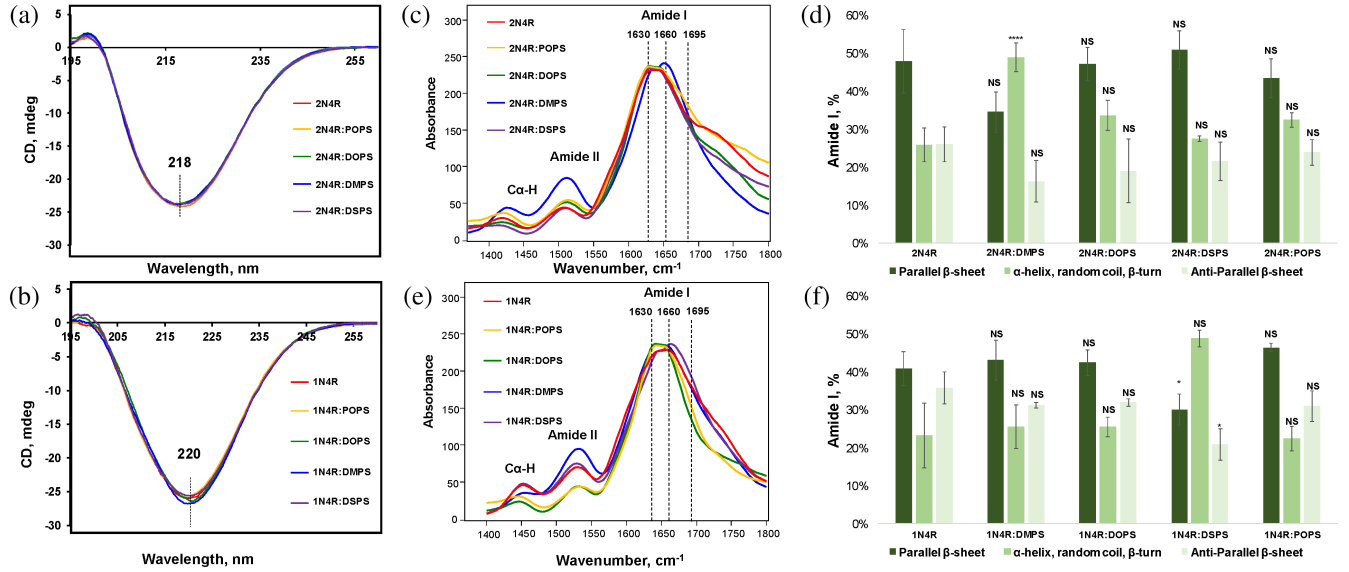

FIGURE 3 Structural characterization of amyloids. CD (a-b) and AFM-IR (c and e) spectra of 2N4R and 1N4R aggregation in lipid-free environment (red), as well as in the presence of POPS (yellow), DOPS (green), DMPS (blue) and DSPS (purple). Histograms (d and f) that summarize distribution of parallel β-sheet, α-helix, random coil and β-turn, as well as anti-parallel β-sheet in the secondary structure of analyzed protein aggregates. According to one-way ANOVA, $*p < 0.05$, $**p < 0.01$, $***p < 0.001$, $****p < 0.0001$. NS shows the absence of statistically significant differences.

protein (∼25%), Figure 3c,d. 2N4R:DOPS, 2N4R:DSPS, and 2N4R:POPS Tau fibrils exhibited very similar secondary structure compared to 2N4R Tau fibrils grown in the lipid-free environment. However, we found significantly higher amount of α-helix and unordered protein (∼50%) in 2N4R:DMPS fibrils, Figure 3c,d. Based on these results, we can conclude that the presence of DMPS causes substantial changes in the secondary structure of 2N4R Tau fibrils. However, the presence of DSPS, DOPS and POPS at the stage of protein aggregation has no effect on the secondary structure of amyloid aggregates.

Nano-IR analysis of 1N4R Tau fibrils revealed substantial differences in their secondary structure compared to the structure of 2N4R Tau fibrils, Figure 3e,f. Specifically, these amyloid aggregates possessed substantially lower amounts of parallel and significantly higher amount of anti-parallel β-sheet compared to 2N4R Tau fibrils. At the same time, the secondary structure of 1N4R:DMPS, 1N4R:DOPS, and 2N4R:POPS Tau fibrils were similar to the secondary structure of 1N4R Tau fibrils formed in the lipid-free environment, Figure 3e,f. However, nano-IR spectroscopy revealed significantly lower amount of both parallel and ant-parallel β-sheet in the secondary structure of 1N4R:DSPS fibrils compared to 1N4R Tau fibrils. Based on these results, we can conclude that the presence of DSPS causes substantial changes in the secondary structure of 1N4R Tau fibrils. However, the presence of DMPS, DOPS and POPS at the stage of protein aggregation has no effect on the secondary structure of amyloid aggregates. Thus, the presence of PS with unsaturated FAs did not cause any changes in the secondary structure of both 1N4R and 2N4R fibrils. At the same time, saturated DMPS and DSPS altered the secondary structure of 2N4R and 1N4R fibrils, respectively. One can expect that these differences between the effects exerted by saturated versus unsaturated FAs of PS on the secondary structure of Tau aggregates is linked to protein–FA interactions. Holman and co-workers previously used computational simulations to examine differences in the binding energies of insulin to FAs with different degrees of saturation (Holman et al., 2023). It was found that the presence of double bounds in FAs strongly altered energies of insulin–FAs interactions. We infer that such differences in binding energies are linked to dissimilar hydrogen bonding that is taken place between amyloidogenic proteins and FAs.

Toxicity of 2N4R and 1N4R Tau aggregates grown in the presence of POPS, DOPS, DMPS and DSPS, as well as in the lipid-free environment.

The question to ask is whether the presence of PS at the stage of protein aggregation alters the toxicity 2N4R and 1N4R fibrils. To answer this question, we investigate the extent to which protein aggregates formed in the presence of PS with different length and saturation of FAs exert cell toxicity to rat midbrain N27 dopaminergic neurons, Figure 4a.

LDH assay revealed statistically significant difference between the toxicity exerted by 2N4R Tau, 2N4R:DOPS,

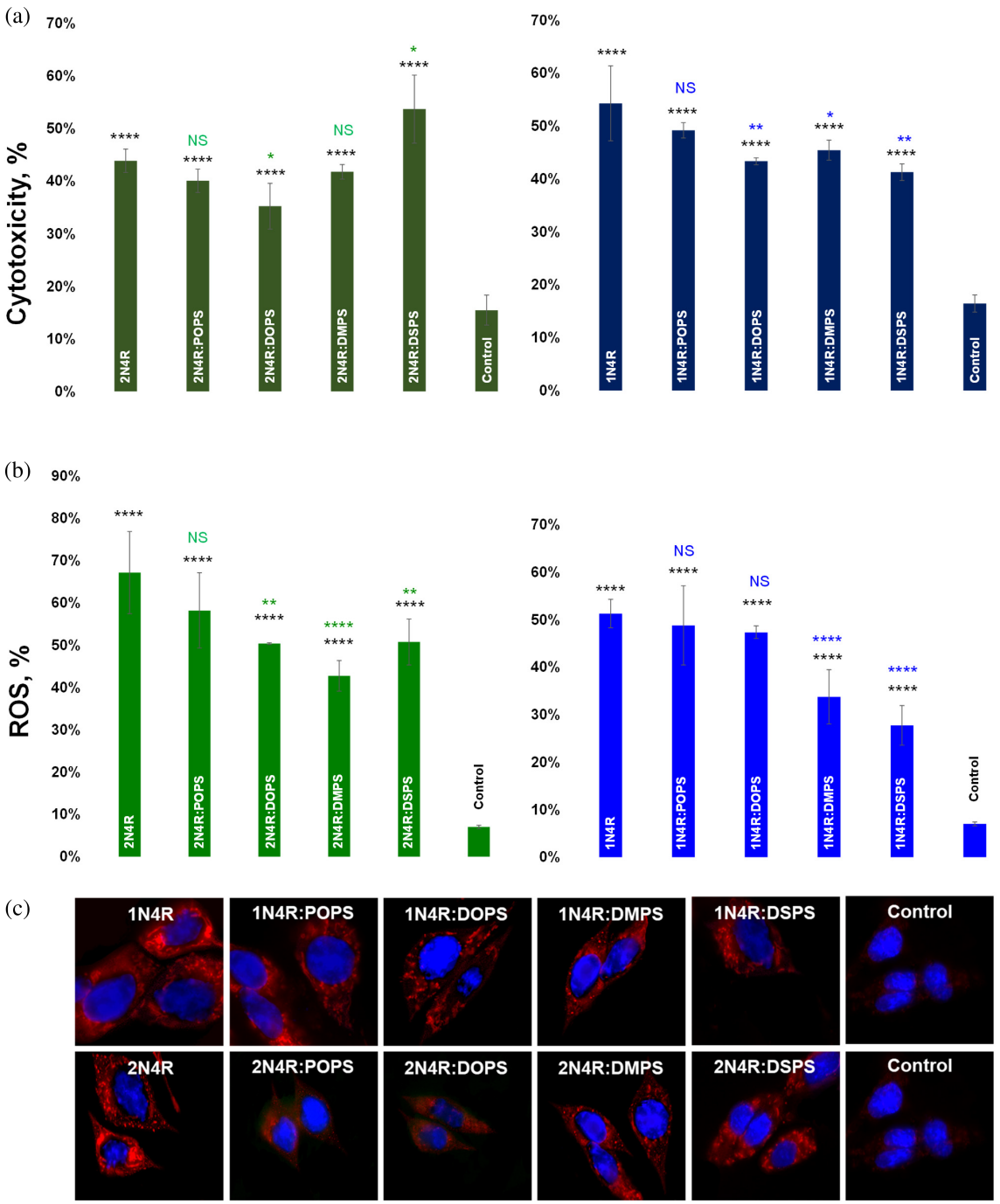

FIGURE 4 Toxicity of Tau aggregates. Histograms of LDH (a) and ROS (b) assays reveal differences between cell toxicity of 2N4R, 2N4R:POPS, 2N4R:DOPS, 2N4R:DMPS, and 2N4R:DSPS (left) and 1N4R, 1N4R:POPS, 1N4R:DOPS, 1N4R:DMPS, and 1N4R:DSPS (right). Black asterisks (*) show significance level of differences between protein aggregates and the control; blue and green asterisks show significance level of difference between protein aggregates formed in the lipid-free environment and in the presence of lipids. According to one-way ANOVA, *$p < 0.05$, **$p < 0.01$, ***$p < 0.001$, ****$p < 0.0001$. NS shows absence of statistical significance. Fluorescence microscopy images (c) show ROS response (red) in the exposed to amyloids N27 cells. The blue fluorescence represents the nuclear fluorescence dye.

and 2N4R:DSPS. Specifically, we found that 2N4R:DOPS fibrils were less and 2N4R:DSPS were more toxic than 2N4R Tau fibrils. We also found that 2N4R:POPS and 2N4R:DMPS fibrils exerted the same levels of cytotoxicity as 2N4R fibrils. Based on these results, we can conclude that the length and saturation of FAs in PS uniquely altered the toxicity of 2N4R fibrils. We also found that 1N4R fibrils were more toxic than 2N4R fibrils. LDH assay revealed that all lipids except POPS decreased the toxicity of 1N4R fibrils. The toxicity of 1N4R and 1N4R:

POPS fibrils were the same. Furthermore, toxicities of 1N4R:DOPS, 1N4R:DMPS, and 1N4R:DSPS Tau were very similar if not identical. Based on these results, we can conclude that PS with saturated FAs lowered the toxicity of 1N4R Tau fibrils, while this effect was not clear for unsaturated versus saturated PS.

We also investigated the extent to which Tau aggregates altered the level of reactive oxygen species (ROS) in N27 rat dopaminergic neurons. We found that all analyzed samples drastically increased the levels of ROS compared to the control, Figure 4b,c. Based on these results, we can conclude that 2N4R and 1N4R Tau aggregates grown in the presence of POPS, DOPS, DMPS and DSPS, as well as in the lipid-free environment caused strong increase in the ROS levels of neurons. We also found that POPS did not alter the ROS levels exerted by both 2N4R and 1N4R fibrils, whereas the presence of both DMPS and DSPS substantially lowered the ROS levels of 2N4R and 1N4R fibrils. The same effect was observed for DOPS in the case of 2N4R, while no changes in the ROS levels exerted by 1N4R fibrils grown in the presence of this lipid were detected. It should be noted that lipids vesicles themselves were not toxic to N27 rat dopaminergic cells, Figure S3 (Ali et al., 2023a, 2023b).

Underlying molecular mechanisms of toxicity of 2N4R and 1N4R Tau aggregates grown in the presence of POPS, DOPS, DMPS and DSPS, as well as in the lipid-free environment.

Endo- and exocytosis of amyloid aggregates cause the spread of AD. In such cases, amyloid oligomers and fibrils present in the intracellular fluid are up taken by healthy cells via endocytosis. As a result, these aggregates are localized in cell endosomes. Previously reported results by our groups showed that insulin aggregates caused severe damage of cell endosomes. This triggered endosomal repair, de novo biogenesis of organelles, and clearance of damaged endosomes by autophagy (Kondow-McConaghy et al., 2020). We utilized a set of biological markers to investigate the extent to which 2N4R and 1N4R Tau aggregates grown in the presence of POPS, DOPS, DMPS and DSPS, as well as in the lipid-free environment caused endosomal damage in HEK 293 T cells.

The magnitude of endosomal damage can be evaluated by the analysis of the expression of Chmp1, a marker protein that binds to membranes of damaged endosomes and activates ESCRT-III complex involved in the membrane repair (Kondow-McConaghy et al., 2020; Radulovic et al., 2018; Skowyra et al., 2018), Figure 5. Endosomal damage also causes a leakage of luminal β-galactosides to the cytosol. Cytosolic Gal3 binds to exposed β-galactosides, initiating autophagy (Kondow-McConaghy et al., 2020; Paz et al., 2010), Figure 5. We transfected HEK 293 T cells with Chmp1-EGFP and Gal3-EGFP constructs and exposed these cells to amyloid aggregates. Next, fluorescence microscopy was utilized to detect and quantify the localization of the expression products of Chmp1-EGFP and Gal3-EGFP. A diffuse and cytosolic distribution of Chmp1/Gal3 is characteristic for healthy cells, while Chmp1/Gal3-EGFP puncta is a hallmark of damaged endosomes.

Endosomal Ca^{2+} efflux also activates TFEB, a transcription factor that regulates lysosomal biogenesis and autophagy (Medina et al., 2015; Sardiello et al., 2009; Settembre et al., 2011). This triggers an activation of the phosphatase calcineurin, dephosphorylation of TFEB, and subsequent translocation of the transcription factor to the nucleus where it activates a transcriptional program that induce de novo biogenesis of endosomal organelles, Figure 5 (Kondow-McConaghy et al., 2020). Therefore, HEK 293T cells transfected with TFEB-EGFP were used to monitor the cytoplasm to nucleus translocation of the transcription factor upon exposure to 2N4R and 1N4R Tau aggregates grown in the presence of POPS, DOPS, DMPS and DSPS, as well as in the lipid-free environment.

Our results indicate that all analyzed protein aggregates caused severe damage to cell endosomes, Figures 5, S4, and S5. We also found that Tau fibrils triggered the endosomal repair, de novo biogenesis of organelles, and clearance of damaged endosomes by autophagy. Based on these results, we can conclude that Tau aggregates are endocytosed by cells. We also found that 2N4R and 1N4R Tau aggregates grown in the presence of POPS, DOPS, DMPS and DSPS, as well as in the lipid-free environment exerted similar magnitudes of endosomal damage. Thus, structural and morphological differences in Tau aggregates have very little if any effect on the extent to which these aggregates alter the magnitude of endosomal repair, de novo biogenesis of organelles, and clearance of damaged endosomes by autophagy. It should be noted that lipids themselves, cause no endosomal damage to the cells, Figure S6.

We hypothesized that amyloid-induced destruction of endosomal membranes will cause a leakage of Tau aggregates into the cytosol where these toxic species can damage mitochondria and endoplasmic reticulum. Expanding upon this, we investigated the extent to which 2N4R and 1N4R Tau aggregates grown in the presence of POPS, DOPS, DMPS and DSPS, as well as in the lipid-free environment caused mitochondrial unfolded protein response (mt-UPR). For this, we utilized qPCR to determine changes in the expression of CLPP, protease enzyme located in the mitochondrial matrix. CLPP is involved in the degradation of misfolded proteins (Al-Furoukh et al., 2015). YME1A is another mitochondrial protease located in the inner MT membrane that facilitates degradation of misfolded proteins (Schreiner et al., 2012).

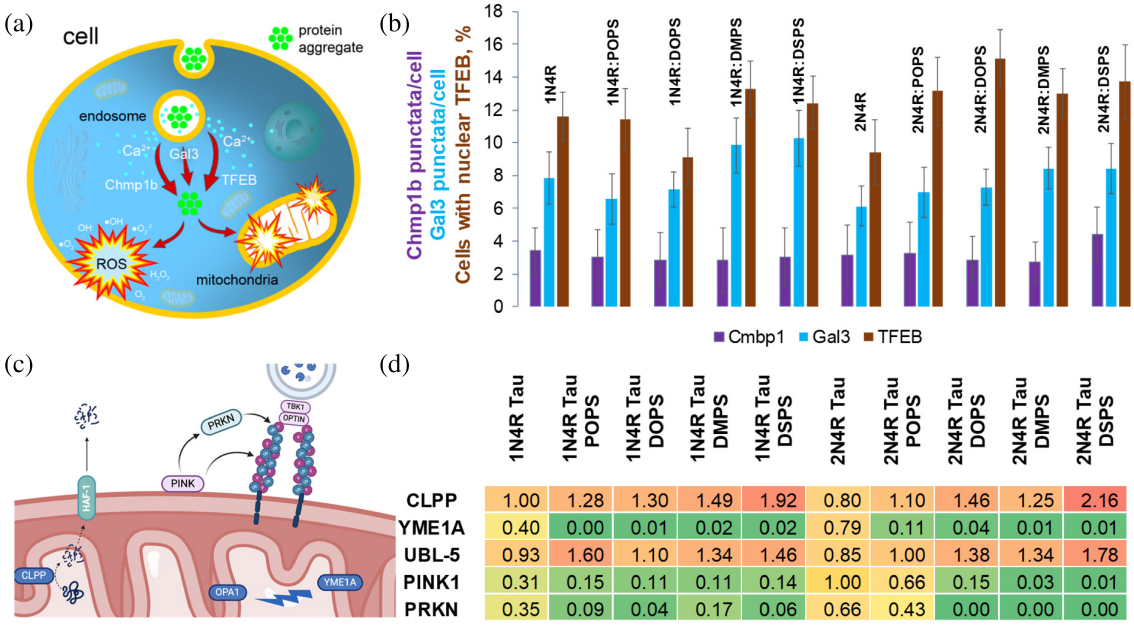

	1N4R Tau	1N4R Tau POPS	1N4R Tau DOPS	1N4R Tau DMPS	1N4R Tau DSPS	2N4R Tau	2N4R Tau POPS	2N4R Tau DOPS	2N4R Tau DMPS	2N4R Tau DSPS
CLPP	1.00	1.28	1.30	1.49	1.92	0.80	1.10	1.46	1.25	2.16
YME1A	0.40	0.00	0.01	0.02	0.02	0.79	0.11	0.04	0.01	0.01
UBL-5	0.93	1.60	1.10	1.34	1.46	0.85	1.00	1.38	1.34	1.78
PINK1	0.31	0.15	0.11	0.11	0.14	1.00	0.66	0.15	0.03	0.01
PRKN	0.35	0.09	0.04	0.17	0.06	0.66	0.43	0.00	0.00	0.00

FIGURE 5 Molecular mechanism of amyloid toxicity. Schematic (a) illustration of endosomal damage induced by Tau aggregates that activate Chmp1b, Gal3, and TFEB factors involved in endosomal repair, clearance of damaged endosomes by autophagy, and de novo biogenesis of organelles, respectively. Histograms (b) of fluorescent puncta per cell, as well as the sum of pixels from fluorescent puncta observed in HEK 293 T cells after their incubation with 2N4R and 1N4R Tau aggregates grown in the presence of POPS, DOPS, DMPS and DSPS, as well as in the lipid-free environment. For each of the presented results, at least 15 individual images were analyzed. Schematic (c) illustration of mitochondrial unfolded protein response (mt-UPR) that activates CLPP, YME1A, UBL-5, PINK1, and PRKN kinases. Heat-map (d) of relative mt-UPR gene expression in N27 rat dopaminergic cells exposed to 2N4R, 2N4R:POPS, 2N4R:DOPS, 2N4R:DMPS, 2N4R:DSPS, 1N4R, 1N4R:POPS, 1N4R:DOPS, 1N4R:DMPS, and 1N4R:DSPS aggregates for 24 h showing a suppression (green), activation (red) or no changes (yellow) in the mt-UPR gene expression.

In addition to CLPP and YME1A, a transcriptional regulator ubiquitin-like protein 5 (UBL-5), plays an important role in mt-UPR. UBL-5 controls the expression of genes responsible for mt-UPR (Broadley & Hartl, 2008). Finally, PTEN-induced kinase 1 (PINK1) and PRKN (Parkin) are involve in mt-UPR. PINK1 senses mt-UPR and membrane damage, which results in the PINK1 accumulation on the exterior side of the mitochondrial membrane. Through auto-phosphorylation, PINK1 activates PRKN, which, in turn, plays an important role in the regulation of mitophagy and degradation of damaged cell mitochondria.

qPCR analysis of expression of proteins involved in mt-UPR revealed a drastic increase in the expression of CLPP and UBL-5 in N27 rat dopaminergic cells exposed to 2N4R and 1N4R Tau aggregates grown in the presence of POPS, DOPS, DMPS and DSPS. However, 2N4R and 1N4R Tau aggregates grown in the lipid-free environment did not cause any significant changes in the expression of CLPP and UBL-5. We also found absence of the increase in the expression of YME1A, PINK1 and PRKN in all analyzed samples. Based on these results, we can conclude that 2N4R and 1N4R Tau aggregates grown in the presence of POPS, DOPS, DMPS and DSPS primarily activated the expression of CLPP and UBL-5, and consequently, damaged cell mitochondria. Our results also showed that 2N4R and 1N4R Tau aggregates grown in the absence of PSs did not cause mt-UPR in N27 rat dopaminergic cells. It should be noted that lipids themselves, cause no changes in the mt-UPR levels, Figure S7.Thus, Tau–PS interactions drastically alter molecular mechanisms by which amyloid aggregates exert their cytotoxicity.

3 | DISCUSSION

Our results indicate that neuronal cells uptake 2N4R and 1N4R Tau aggregates grown in the presence and absence of PS by endocytosis. As a result, protein aggregates accumulate in cell endosomes causing damage of these important cell organelles. This activates mechanisms involved in endosomal repair, de novo biogenesis of organelles, and clearance of damaged endosomes by autophagy (Matveyenka, Rizevsky, et al., 2023). Our results showed that 2N4R and 1N4R Tau aggregates grown in the presence and absence of PS with different length and saturation of FAs exert highly similar if not identical magnitude of endosomal damage. At the same time,

previously reported results by our group demonstrated that insulin aggregates with drastically different secondary structures exerted significantly different magnitudes of endosomal damage to N27 rat dopaminergic cells (Matveyenka, Rizevsky, et al., 2023). These findings are in good agreement with our CD and nano-IR results which revealed minor changes in the secondary structure of 2N4R and 1N4R Tau aggregates grown in the presence and absence of PS.

We also found that the length and saturation of FAs in PS uniquely altered the morphology and toxicity of both 1N4R and 2N4R Tau fibrils. These findings are consistent with previously reported by our group results for α-syn, TTR and insulin (Ali et al., 2023a; Ali et al., 2023b; Ali et al., 2023c; Matveyenka, Rizevsky, et al., 2023). Based on these findings, we can conclude that morphology and toxicity of amyloid aggregates is to a large extent determined by the length and saturation of FAs in PS. In our previous study, we investigated molecular mechanisms that determine FA-induced differences in the morphology of protein aggregates (Holman et al., 2023). We found that saturation of FAs alters protein–lipid interactions, which, in turn, play an important role in the protein aggregation (Holman et al., 2023). These results are also consistent with experimental findings reported by Mezzenga's group (Adamcik et al., 2010; Ke et al., 2020). Using AFM, the researchers proposed that fibril morphology is determined by a balance between free energy minimization and electrostatic repulsion (Diener et al., 2020; Sanchez-Ferrer et al., 2018). Free energy force aims makes fibril twist, whereas electrostatic repulsion, which appears as a result of the extensive twist of such fibrils, prevents supercoiling of amyloid aggregates. Consequently, the presence of lipids in such fibrils, as was revealed by cryo-EM (Frieg et al., 2022; Frieg et al., 2024), alters electrostatic forces and, consequently, fibril morphology. It should be noted that observed 1N4R and 2N4R Tau fibrils were dominated by parallel β-sheet, which points on their high stability to changing environmental factors (Kurouski et al., 2010; Shanmugasundaram et al., 2015).

Our results also revealed differences in the rates of 2N4R Tau aggregation in the presence of PS with different length and saturation of FAs. Similar findings were previously reported by Ali and co-workers for α-syn and TTR (Ali et al., 2023a; Ali et al., 2023b; Ali et al., 2023c). Specifically, it was shown that length and saturation of FAs uniquely altered the aggregation rate of these proteins. Our results also indicated that that such effect was entirely absent in 1N4R Tau. Based on these results, we can conclude that 2 N terminal insert plays an important role in protein–lipid interactions, Scheme 1. Additional studies that will employ site-specific mutagenesis and computational simulations are required to make more specific conclusions about the role of individual amino acid present in 2 N insert in such protein–lipid interactions. This information can be critically important for the development of novel therapeutic approaches that will inhibit Tau–lipid interactions, and consequently, alter the aggregation properties of Tau proteins in AD brains.

We observed a direct relationship between ROS levels exerted by 1N4R Tau fibrils formed in the presence and absence of lipids and their cytoxicity probed by LDH assay. These results indicate that ROS triggered by 1N4R Tau aggregates are likely to be the major cause of their cytotoxicity. These results are further supported by highly similar endosomal damage exerted by all of 1N4R Tau fibrils formed in the presence and absence of lipids. However, only partial correlation was observed for 2N4R Tau fibrils. Specifically, we found that ROS and LDH levels correlate for 2N4R:POPS Tau and 2N4R:DOPS Tau, whereas no correlation was observed for 2N4R Tau fibrils formed in the presene of PS with saturated FAs. These results indicate that other molecular mechanisms are involved in cytoxicity exerted by 2N4R:DMPS Tau and 2N4R:DSPS Tau fibrils.

4 | CONCLUSIONS

Our results demonstrate that PS with different length and saturation of FAs present at the stage of protein aggregation uniquely altered the aggregation rates of 2N4R Tau isoform, whereas no changes in the aggregation rate of 1N4R were observed. These results indicate that 2 N terminal insert plays an important role in Tau–lipid interactions. Our findings also show that Tau fibrils formed in the presence and absence of PS endocytosed by cells. This causes severe damage of cell endosomes and leakage of toxic amyloid aggregates in the cytosol where they enhance ROS levels and exert strong impairment of the cell mitochondria. Our results also demonstrated that the length and saturation of FAs in PS uniquely altered the morphology and toxicity of Tau fibrils. Thus, Tau–PS interactions, which may likely happen in the brains of AD patients can strongly alter protein stability and yield amyloid oligomers and fibrils with drastically different cytotoxicity compare to the amyloid aggregates formed in the lipid-free environment.

5 | EXPERIMENTAL SECTION

5.1 | Materials

DMPS, 1,2-dioleoyl-sn-glycero-3-phospho-L-serine (DOPS), 1-palmitoyl-2-oleoyl-sn-glycero-3-phospho-

L-serine (POPS) and 1,2-distearyl-sn-glycero-3-phospho-L-serine (DSPS) were purchased from Avanti (Alabaster, AL, USA), IPTG was purchased from SIGMA USA.

5.2 | Liposome preparation

To prepare LUVs of DMPS, DSPS, POPS, and DOPS, 0.6 mg of each lipid was dissolved in 2.6 ml of phosphate buffered saline (PBS), pH 7.4. Lipid solutions were then first heated ~50°C for 30 min in a water bath. After that, samples were immersed into liquid nitrogen for 3–5 min. The thawing-heating cycle was repeated 10 times. To homogenize the size of lipid vesicles, lipid solutions were at the end passed through 100 nm membrane using extruder (Avanti, Alabaster, AL). Such LUVs have spherical shapes (Dou et al., 2022). Finally, we utilized dynamic light scattering to ensure that the size of the LUVs was within 100 ± 10 nm.

5.3 | Protein expression and purification Tau 2N4R and 1N4R

The proteins pET28B-Tau2N4R and pET28B-Tau1N4R were subjected to overexpression in Escherichia coli BL21 (DE3) Rosetta strain utilizing LB broth media. A total of six liters of bacterial culture, with an optical density (OD) reading of 0.9, was induced with 1 mM Isopropyl β-D-1-thiogalactopyranoside (IPTG) and allowed to incubate at 16°C overnight. Upon reaching the desired induction period, the overnight cultures were subjected to centrifugation at 8000 RPM for 10 min, resulting in the formation of a pellet. This pellet was subsequently re-suspended in lysis buffer consisting of 8 M Urea, 50 mM Tris–HCl, 50 mM NaCl, pH 8.0, supplemented with a protease inhibitor cocktail containing 100 mM Phenylmethylsulfonyl fluoride (PMSF). The re-suspended culture underwent a cycle of freeze–thaw followed by sonication at 28% Amplitude. Following sonication, the samples were centrifuged at 16,000 g for 1 h to separate the soluble fraction, and the resulting supernatants were carefully collected. To ensure the removal of any particulate matter, the supernatants were passed through a syringe filter with a pore size of 0.4 μm. The filtered supernatants were then subjected to affinity chromatography using Ni-NTA agarose beads within a gravity column setup. Prior to elution, the column was washed extensively with a washing buffer comprising 50 mM Tris–HCl, 300 mM NaCl, and 20 mM Imidazole, to remove non-specifically bound proteins. Subsequently, the target proteins were eluted from the column using an elution buffer containing 50 mM Tris–HCl, 300 mM NaCl, and 300 mM Imidazole, in a total volume of 50 mL. The eluted protein fractions were then dialyzed against PBS (pH 7.4) using a dialysis membrane with a molecular weight cut-off of 30 kDa to remove urea and imidazole. Post-dialysis, protein samples were concentrated using centrifugal concentrators with a 30 kDa molecular weight cut-off. The final concentration of the purified protein was determined to be ~2.5 mg/mL. To assess the purity and size of the obtained proteins, Sodium Dodecyl Sulfate Polyacrylamide Gel Electrophoresis (SDS-PAGE) analysis was performed (Figure S8).

5.4 | 2N4R and 1N4R Tau aggregation

In the lipid-free environment, 100 μM of protein was dissolved in PBS that contained 30 μM of heparin; the solution pH was adjusted to pH 7.4. For 2N4R and 1N4R Tau aggregation in the presence of PS, 100 μM of protein was mixed with 30 μM of heparin and an equivalent concentration of the corresponding LUVs; the pH of the final solution was adjusted to pH 7.4 using concentrated HCl. Next, samples were placed into 96 well-plate that was kept in the plate reader (Tecan, Männedorf, Switzerland) at 37°C for 150 h under 510 rpm agitation.

5.5 | Kinetic measurements

Rates of protein aggregation were measured using thioflavin T (ThT) fluorescence assay. For this, samples were mixed with 2 mM of ThT solution and placed into 96 well-plate that was kept in the plate reader (Tecan, Männedorf, Switzerland) at 37°C for 150 h under 510 rpm agitation. Fluorescence measurements were taken every 10 min (excitation 450 nm; emission 488 nm). Each kinetic curve is an average of four independent measurements.

5.6 | Atomic force microscopy (AFM) imaging

AIST-NT-HORIBA system (Edison, NJ) AFM system was utilized to perform topological characterization of Tau aggregates. Tapping-mode AFM probes Appnano (Mountain View, CA, USA) were used with force constant of 2.7 N/m and resonance frequency of 50–80 kHz. Sample was first diluted with DI water and then placed on the surface of pre-cleaned glass coverslip. Pre-

processing of the collected AFM images was made using AIST-NT software (Edison, NJ).

5.7 | Atomic force microscopy infrared spectroscopy

Protein samples were deposited on a 70 nm gold-coated silicon wafer. After the samples were exposed on the wafer surface for ~20 min, the excess solutions were removed; the wafers were dried at room temperature. Next, the wafer surface was rinsed with DI water and again dried under N_2 flow. AFM-IR imaging was conducted using a Nano-IR3 system (Bruker, Santa Barbara, CA). The IR source was a QCL laser. Contact-mode AFM tips (ContGB-G AFM probe, NanoAndMore) were used to acquire AFM-IR spectra. No evidence of the sample distortion was observed upon contact-mode AFM imaging. The contact-mode tip was optimized using a polymethyl methacrylate standard sample in 1400–1800 cm^{-1}. Totally, 20 point measurements were taken from every analyzed sample. The spectra were zapped from 1648 to 1652 cm^{-1} to remove the artifact originating from the chip-to-chip transition. The spectra resolution is 2 cm^{-1}/pt. Savitzky–Golay smoothing was applied to all spectra with two polynomial orders by using MATLAB.

5.8 | Circular dichroism

Samples were first diluted to the final concentration of 100 μM using PBS and measured immediately using Jasco J1000 CD spectrometer (Jasco, Easton, MD). Three spectra were collected for each sample within 195–250 nm and averaged.

5.9 | Cell toxicity assays

Rat midbrain N27 cells were grown in RPMI 1640 Medium (Thermo Fisher Scientific, Waltham, MA, USA) with 10% fetal bovine serum (FBS) (Invitrogen, Waltham, MA, USA) in 96 well-plate (5000 cells per well) at 37°C under 5% CO_2. After 24 h, the cells were found to fully adhere to the wells reaching ~70% confluency. Next, 100 μL of the cell culture was replaced with 100 μL RPMI 1640 Medium with 5% FBS containing protein samples that were incubated at 37°C for 150 h under 510 rpm agitation. Final concentration of protein aggregates was 30 μM. After 24 h of incubation with the sample of the protein aggregates, lactate dehydrogenase (LDH) assay (G1781, Promega, Madison, WI, USA) that was used to determine toxicity of protein aggregates. Absorption measurements were made in plate reader (Tecan, Mannedorf, Switzerland) at 490 nm. Every well was measured 25 times in different locations. All experiments were made in triplicates.

In parallel, reactive oxygen species (ROS) assay was performed using the same cell culture. ROS reagent (C10422, Invitrogen, Waltham, MA, USA) was added to reach the final concentration of 5 μM and incubated at 37°C under 5% CO_2 for 30 min. After the supernatant was removed, cells were washed with PBS and resuspended in 200 μL of PBS in the flow cytometry tubes. Sample measure-ments were made in LSRII Flow Cytometer (BD, San Jose, CA, USA) using red channel ($\lambda = 633$ nm). Percentages of ROS cells were determined using Acura software. All experiments were made in triplicates.

5.10 | Fluorescence microscopy

N27 rat dopaminergic neuron cells were cultured in RPMI 1640 Medium (Thermo Fisher Scientific) supplemented with 10% fetal bovine serum (FBS) (Invitrogen, Waltham, MA) in 35 mm dishes with optical bottoms (Cat. No. D35–10 − 1.5-N, Cellvis), with 300,000 cells per well, and maintained at 37°C in a 5% CO_2 environment. After 24 h, cell culture medium was replaced with fresh RPMI 1640 Medium containing 5% FBS and including the protein samples that were incubated at 37°C for 150 h under 510 rpm agitation. Final concentration of protein aggregates was 30 μM. After 24 h of incubation, ROS reagent was added to achieve final concentrations of 5 μM. Cells were incubated for 20 min at 37°C in a 5% CO_2. Next, one drop of NucBlue Live Cell ReadyProbes (Cat. No. R37605, Invitrogen) was added to each sample and incubated for 5 min at 37°C in a 5% CO_2. Fluorescence images were taken on EVOS M5000 Imaging System (Invitrogen) with an Olympus UPIanApo 100x/1.35 oil iris ∞/0.17 objective and blue, deep red, and green filters. All experiments were made in triplicates.

5.11 | Membrane leakage assay

Plasmids that code Chmp1b (cell membrane repair), Gal3 (autophagy) and TFEB (lysosome biogenesis) were delivered in HEK 293 T cell using GeneX Plus reagent (ACS-4004, ATCC, Manassas, VA, USA). HET 293 T cells were grown in Dulbecco's Modified Eagle Medium (DMEM) cell medium that contained 10% FBS. After 24 h, cells were found to fully adhere to the wells reaching ~80% confluency. Cell transfection was performed in DMEM that contained no FBS for 4 h. After that, cell media was

replaced on DMEM with 10% FBS and incubated for 24 h at 37°C in a 5% CO_2. Next, amyloid aggregates that were formed at 37°C for 150 h under 510 rpm agitation were added to HET 293 T cells and incubated for 24 h at 37°C in a 5% CO_2. Final concentration of protein aggregates was 30 μM. Fluorescence imaging was performed in EVOS M5000 microscope (Thermo Fisher Scientific, Waltham, MA, USA). Chmp1b and TFEB plasmids contain green fluorescence protein and Gal3 contains red fluorescence protein, Figures S1 and S2. Microscopic images reported in Figure S1 and S2 show cells with various numbers of punctata present in each cell. Using these images, we counted the number of punctata in cells treated with insulin aggregates grown in the presence and absence of lipids. All experiments were made in triplicates.

5.12 | Gene expression

RNA was first extracted from N27 rat dopaminergic cells exposed to amyloids that were formed at 37°C for 150 h under 510 rpm agitation for 24 h using GeneJET RNA Purification Kit (catalog no. K0732, Thermo Scientific). Final concentration of protein aggregates was 30 μM. The concentration of extracted RNA was determined using a NanoDrop One instrument (Thermo Scientific). cDNA synthesis was performed using SuperScript III Reverse Transcriptase (catalog no. 18080093, Invitrogen) with random primers (catalog no. 48190011, Invitrogen). Specific primers were designed for each target gene (Zhaliazka et al., 2024). qPCR was performed on C1000 Touch Thermal Cycler (BioRad) for 35–40 cycles. Each reaction mixture contained a cDNA, primers, and SYBR Green PCR master mix (Cat. No. 4309155, Applied Biosystems). β-Actin was used as a housekeeping gene to normalize the expression levels of the target genes. Nontemplate controls and positive controls were included in each qPCR run to ensure the accuracy and reliability of the results. All experiments were made in triplicates.

5.13 | Data analysis

The quantification of relative gene expression was determined using the comparative Ct method ($2^{-\Delta\Delta Ct}$), where ΔCt represents the difference in threshold cycles between the target gene and the housekeeping gene and ΔΔCt represents the difference in ΔCt values between the treated samples and the control samples. The relative gene expression levels were calculated and presented as fold changes compared with the control samples.

AUTHOR CONTRIBUTIONS

Abid Ali: Investigation; conceptualization; methodology; validation; writing – review and editing. **Aidan P. Holman:** Conceptualization; investigation; methodology; validation; writing – review and editing. **Axell Rodriguez:** Conceptualization; investigation; methodology; validation; writing – review and editing. **Mikhail Matveyenka:** Conceptualization; investigation; methodology; validation; writing – review and editing. **Dmitry Kurouski:** Conceptualization; funding acquisition; writing – original draft; writing – review and editing; visualization; project administration; resources; supervision.

ACKNOWLEDGMENTS

We are grateful to the National Institute of General Medical Sciences for the provided financial support (R35GM142869).

ORCID

Dmitry Kurouski https://orcid.org/0000-0002-6040-4213

REFERENCES

Adamcik J, Jung JM, Flakowski J, de Los Rios P, Dietler G, Mezzenga R. Understanding amyloid aggregation by statistical analysis of atomic force microscopy images. Nat Nanotechnol. 2010;5:423–8. https://doi.org/10.1038/nnano.2010.59

Ait-Bouziad N, Lv G, Mahul-Mellier AL, Xiao S, Zorludemir G, Eliezer D, et al. Discovery and characterization of stable and toxic tau/phospholipid oligomeric complexes. Nat Commun. 2017;8:1678. https://doi.org/10.1038/s41467-017-01575-4

Alecu I, Bennett SAL. Dysregulated lipid metabolism and its role in alpha-Synucleinopathy in Parkinson's disease. Front Neurosci. 2019;13:328. https://doi.org/10.3389/fnins.2019.00328

Al-Furoukh N, Ianni A, Nolte H, Holper S, Kruger M, Wanrooij S, et al. ClpX stimulates the mitochondrial unfolded protein response (UPRmt) in mammalian cells. Biochim Biophys Acta. 2015;1853:2580–91. https://doi.org/10.1016/j.bbamcr.2015.06.016

Ali A, Zhaliazka K, Dou T, Holman AP, Kurouski D. Role of saturation and length of fatty acids of phosphatidylserine in the aggregation of transthyretin. ACS Chem Neurosci. 2023a;14:3499–506. https://doi.org/10.1021/acschemneuro.3c00357

Ali A, Zhaliazka K, Dou T, Holman AP, Kurouski D. The toxicities of A30P and A53T alpha-synuclein fibrils can be uniquely altered by the length and saturation of fatty acids in phosphatidylserine. J Biol Chem. 2023b;299:105383. https://doi.org/10.1016/j.jbc.2023.105383

Ali A, Zhaliazka K, Dou T, Holman AP, Kurouski D. Saturation of fatty acids in phosphatidic acid uniquely alters transthyretin stability changing morphology and toxicity of amyloid fibrils. Chem Phys Lipids. 2023c;257:105350. https://doi.org/10.1016/j.chemphyslip.2023.105350

Alonso AD, Zaidi T, Novak M, Barra HS, Grundke-Iqbal I, Iqbal K. Interaction of tau isoforms with Alzheimer's disease abnormally hyperphosphorylated tau and in vitro phosphorylation

into the disease-like protein. J Biol Chem. 2001;276:37967–73. https://doi.org/10.1074/jbc.M105365200

Alonso Adel C, Mederlyova A, Novak M, Grundke-Iqbal I, Iqbal K. Promotion of hyperphosphorylation by frontotemporal dementia tau mutations. J Biol Chem. 2004;279:34873–81. https://doi.org/10.1074/jbc.M405131200

Bodner CR, Dobson CM, Bax A. Multiple tight phospholipid-binding modes of α-synuclein revealed by solution NMR spectroscopy. J Mol Biol. 2009;390:775–90. https://doi.org/10.1016/j.jmb.2009.05.066

Bodner CR, Maltsev AS, Dobson CM, Bax A. Differential phospholipid binding of α-synuclein variants implicated in Parkinson's disease revealed by solution NMR spectroscopy. Biochemistry. 2010;49:862–71. https://doi.org/10.1021/bi901723p

Broadley SA, Hartl FU. Mitochondrial stress signaling: a pathway unfolds. Trends Cell Biol. 2008;18:1–4. https://doi.org/10.1016/j.tcb.2007.11.003

Clavaguera F, Bolmont T, Crowther RA, Abramowski D, Frank S, Probst A, et al. Transmission and spreading of tauopathy in transgenic mouse brain. Nat Cell Biol. 2009;11:909–13. https://doi.org/10.1038/ncb1901

Diener M, Adamcik J, Bergfreund J, Catalini S, Fischer P, Mezzenga R. Rigid, fibrillar quaternary structures induced by divalent ions in a Carboxylated linear polysaccharide. ACS Macro Lett. 2020;9:115–21. https://doi.org/10.1021/acsmacrolett.9b00824

Dou T, Kurouski D. Phosphatidylcholine and phosphatidylserine uniquely modify the secondary structure of alpha-synuclein oligomers formed in their presence at the early stages of protein aggregation. ACS Chem Neurosci. 2022;13:2380–5. https://doi.org/10.1021/acschemneuro.2c00355

Dou T, Matveyenka M, Kurouski D. Elucidation of secondary structure and toxicity of alpha-synuclein oligomers and fibrils grown in the presence of phosphatidylcholine and phosphatidylserine. ACS Chem Neurosci. 2023;14:3183–91. https://doi.org/10.1021/acschemneuro.3c00314

Dou T, Zens C, Schroder K, Jiang Y, Makarov AA, Kupfer S, et al. Solid-to-liposome conformational transition of phosphatidylcholine and phosphatidylserine probed by atomic force microscopy, infrared spectroscopy, and density functional theory calculations. Anal Chem. 2022;94:13243–9. https://doi.org/10.1021/acs.analchem.2c03061

Dou T, Zhou L, Kurouski D. Unravelling the structural Organization of Individual alpha-synuclein oligomers grown in the presence of phospholipids. J Phys Chem Lett. 2021;12:4407–14. https://doi.org/10.1021/acs.jpclett.1c00820

Eisenberg DS, Sawaya MR. Neurodegeneration: taming tangled tau. Nature. 2017;547:170–1. https://doi.org/10.1038/nature23094

Falcon B, Zivanov J, Zhang W, Murzin AG, Garringer HJ, Vidal R, et al. Novel tau filament fold in chronic traumatic encephalopathy encloses hydrophobic molecules. Nature. 2019;568:420–3. https://doi.org/10.1038/s41586-019-1026-5

Fitzner D, Bader JM, Penkert H, Bergner CG, Su M, Weil MT, et al. Cell-type- and brain-region-resolved mouse brain lipidome. Cell Rep. 2020;32:108132. https://doi.org/10.1016/j.celrep.2020.108132

Frieg B, Antonschmidt L, Dienemann C, Geraets JA, Najbauer EE, Matthes D, et al. The 3D structure of lipidic fibrils of alpha-synuclein. Nat Commun. 2022;13:6810. https://doi.org/10.1038/s41467-022-34552-7

Frieg B, Han M, Giller K, Dienemann C, Riedel D, Becker S, et al. Cryo-EM structures of lipidic fibrils of amyloid-beta (1-40). Nat Commun. 2024;15:1297. https://doi.org/10.1038/s41467-023-43822-x

Giamblanco N, Fichou Y, Janot JM, Balanzat E, Han S, Balme S. Mechanisms of heparin-induced tau aggregation revealed by a single nanopore. ACS Sens. 2020;5:1158–67. https://doi.org/10.1021/acssensors.0c00193

Goedert M, Spillantini MG, Jakes R, Rutherford D, Crowther RA. Multiple isoforms of human microtubule-associated protein tau: sequences and localization in neurofibrillary tangles of Alzheimer's disease. Neuron. 1989;3:519–26. https://doi.org/10.1016/0896-6273(89)90210-9

Gouras GK, Tampellini D, Takahashi RH, Capetillo-Zarate E. Intraneuronal beta-amyloid accumulation and synapse pathology in Alzheimer's disease. Acta Neuropathol. 2010;119:523–41. https://doi.org/10.1007/s00401-010-0679-9

Grundke-Iqbal I, Iqbal K, Tung YC, Quinlan M, Wisniewski HM, Binder LI. Abnormal phosphorylation of the microtubule-associated protein tau (tau) in Alzheimer cytoskeletal pathology. Proc Natl Acad Sci U S A. 1986;83:4913–7. https://doi.org/10.1073/pnas.83.13.4913

Himmler A, Drechsel D, Kirschner MW, Martin DW Jr. Tau consists of a set of proteins with repeated C-terminal microtubule-binding domains and variable N-terminal domains. Mol Cell Biol. 1989;9:1381–8. https://doi.org/10.1128/mcb.9.4.1381-1388.1989

Holman AP, Quinn K, Kumar R, Kmiecik S, Ali A, Kurouski D. Fatty acids reverse the supramolecular chirality of insulin fibrils. J Phys Chem Lett. 2023;14:6935–9. https://doi.org/10.1021/acs.jpclett.3c01527

Karikari TK, Nagel DA, Grainger A, Clarke-Bland C, Hill EJ, Moffat KG. Preparation of stable tau oligomers for cellular and biochemical studies. Anal Biochem. 2019;566:67–74. https://doi.org/10.1016/j.ab.2018.10.013

Ke PC, Zhou R, Serpell LC, Riek R, Knowles TPJ, Lashuel HA, et al. Half a century of amyloids: past, present and future. Chem Soc Rev. 2020;49:5473–509. https://doi.org/10.1039/c9cs00199a

Kondow-McConaghy HM, Muthukrishnan N, Erazo-Oliveras A, Najjar K, Juliano RL, Pellois JP. Impact of the endosomal escape activity of cell-penetrating peptides on the endocytic pathway. ACS Chem Biol. 2020;15:2355–63. https://doi.org/10.1021/acschembio.0c00319

Kurouski D, Lauro W, Lednev IK. Amyloid fibrils are "alive": spontaneous refolding from one polymorph to another. Chem Commun (Camb). 2010;46:4249–51. https://doi.org/10.1039/b926758a

LaPointe NE, Morfini G, Pigino G, Gaisina IN, Kozikowski AP, Binder LI, et al. The amino terminus of tau inhibits kinesin-dependent axonal transport: implications for filament toxicity. J Neurosci Res. 2009;87:440–51. https://doi.org/10.1002/jnr.21850

Lasagna-Reeves CA, Castillo-Carranza DL, Jackson GR, Kayed R. Tau oligomers as potential targets for immunotherapy for Alzheimer's disease and tauopathies. Curr Alzheimer Res. 2011;8:659–65. https://doi.org/10.2174/156720511796717177

Lasagna-Reeves CA, Castillo-Carranza DL, Sengupta U, Clos AL, Jackson GR, Kayed R. Tau oligomers impair memory and induce synaptic and mitochondrial dysfunction in wild-type mice. Mol Neurodegener. 2011;6:39. https://doi.org/10.1186/1750-1326-6-39

Lasagna-Reeves CA, Castillo-Carranza DL, Sengupta U, Guerrero-Munoz MJ, Kiritoshi T, Neugebauer V, et al. Alzheimer brain-derived tau oligomers propagate pathology from endogenous tau. Sci Rep. 2012;2:700. https://doi.org/10.1038/srep00700

Lasagna-Reeves CA, Castillo-Carranza DL, Sengupta U, Sarmiento J, Troncoso J, Jackson GR, et al. Identification of oligomers at early stages of tau aggregation in Alzheimer's disease. FASEB J. 2012;26:1946–59. https://doi.org/10.1096/fj.11-199851

Levental I, Levental KR, Heberle FA. Lipid rafts: controversies resolved. Mysteries Remain Trends Cell Biol. 2020;30:341–53. https://doi.org/10.1016/j.tcb.2020.01.009

Maltsev AS, Chen J, Levine RL, Bax A. Site-specific interaction between α-synuclein and membranes probed by NMR-observed methionine oxidation rates. J Am Chem Soc. 2013;135:2943–6. https://doi.org/10.1021/ja312415q

Matveyenka M, Rizevsky S, Kurouski D. The degree of unsaturation of fatty acids in phosphatidylserine alters the rate of insulin aggregation and the structure and toxicity of amyloid aggregates. FEBS Lett. 2022;596:1424–33. https://doi.org/10.1002/1873-3468.14369

Matveyenka M, Rizevsky S, Pellois JP, Kurouski D. Lipids uniquely alter rates of insulin aggregation and lower toxicity of amyloid aggregates. Biochim Biophys Acta Mol Cell Biol Lipids. 2023;1868:159247. https://doi.org/10.1016/j.bbalip.2022.159247

Matveyenka M, Zhaliazka K, Kurouski D. Concentration of phosphatidylserine influence rates of insulin aggregation and toxicity of amyloid aggregates in vitro. ACS Chem Neurosci. 2023;14:2396–404. https://doi.org/10.1021/acschemneuro.3c00277

McLean CA, Cherny RA, Fraser FW, Fuller SJ, Smith MJ, Beyreuther K, et al. Soluble pool of Abeta amyloid as a determinant of severity of neurodegeneration in Alzheimer's disease. Ann Neurol. 1999;46:860–6. https://doi.org/10.1002/1531-8249(199912)46:6<860::aid-ana8>3.0.co;2-m

Medina DL, di Paola S, Peluso I, Armani A, de Stefani D, Venditti R, et al. Lysosomal calcium signalling regulates autophagy through calcineurin and TFEB. Nat Cell Biol. 2015;17:288–99. https://doi.org/10.1038/ncb3114

Morfini GA, Burns M, Binder LI, Kanaan NM, LaPointe N, Bosco DA, et al. Axonal transport defects in neurodegenerative diseases. J Neurosci. 2009;29:12776–86. https://doi.org/10.1523/JNEUROSCI.3463-09.2009

Nath S, Agholme L, Kurudenkandy FR, Granseth B, Marcusson J, Hallbeck M. Spreading of neurodegenerative pathology via neuron-to-neuron transmission of beta-amyloid. J Neurosci. 2012;32:8767–77. https://doi.org/10.1523/JNEUROSCI.0615-12.2012

Paz I, Sachse M, Dupont N, Mounier J, Cederfur C, Enninga J, et al. Galectin-3, a marker for vacuole lysis by invasive pathogens. Cell Microbiol. 2010;12:530–44. https://doi.org/10.1111/j.1462-5822.2009.01415.x

Radulovic M, Schink KO, Wenzel EM, Nahse V, Bongiovanni A, Lafont F, et al. ESCRT-mediated lysosome repair precedes lysophagy and promotes cell survival. EMBO J. 2018;37:e99753. https://doi.org/10.15252/embj.201899753

Rajendran L, Honsho M, Zahn TR, Keller P, Geiger KD, Verkade P, et al. Alzheimer's disease beta-amyloid peptides are released in association with exosomes. Proc Natl Acad Sci U S A. 2006;103:11172–7. https://doi.org/10.1073/pnas.0603838103

Sanchez-Ferrer A, Adamcik J, Handschin S, Hiew SH, Miserez A, Mezzenga R. Controlling supramolecular chiral nanostructures by self-assembly of a biomimetic beta-sheet-rich amyloidogenic peptide. ACS Nano. 2018;12:9152–61. https://doi.org/10.1021/acsnano.8b03582

Sardiello M, Palmieri M, di Ronza A, Medina DL, Valenza M, Gennarino VA, et al. A gene network regulating lysosomal biogenesis and function. Science. 2009;325:473–7. https://doi.org/10.1126/science.1174447

Schreiner B, Westerburg H, Forne I, Imhof A, Neupert W, Mokranjac D. Role of the AAA protease Yme1 in folding of proteins in the intermembrane space of mitochondria. Mol Biol Cell. 2012;23:4335–46. https://doi.org/10.1091/mbc.E12-05-0420

Settembre C, Di Malta C, Polito VA, Garcia Arencibia M, Vetrini F, Erdin S, et al. TFEB links autophagy to lysosomal biogenesis. Science. 2011;332:1429–33. https://doi.org/10.1126/science.1204592

Shafiei SS, Guerrero-Munoz MJ, Castillo-Carranza DL. Tau oligomers: cytotoxicity, propagation, and mitochondrial damage. Front Aging Neurosci. 2017;9:83. https://doi.org/10.3389/fnagi.2017.00083

Shanmugasundaram M, Kurouski D, Wan W, Stubbs G, Dukor RK, Nafie LA, et al. Rapid filament supramolecular chirality reversal of HET-s (218-289) prion fibrils driven by pH elevation. J Phys Chem B. 2015;119:8521–5. https://doi.org/10.1021/acs.jpcb.5b04779

Skowyra ML, Schlesinger PH, Naismith TV, Hanson PI. Triggered recruitment of ESCRT machinery promotes endolysosomal repair. Science. 2018;360:eaar5078. https://doi.org/10.1126/science.aar5078

Takashima A. Tauopathies and tau oligomers. J Alzheimers Dis. 2013;37:565–8. https://doi.org/10.3233/JAD-130653

Wang Y, Balaji V, Kaniyappan S, Kruger L, Irsen S, Tepper K, et al. The release and trans-synaptic transmission of tau via exosomes. Mol Neurodegener. 2017;12:5. https://doi.org/10.1186/s13024-016-0143-y

Weingarten MD, Lockwood AH, Hwo SY, Kirschner MW. A protein factor essential for microtubule assembly. Proc Natl Acad Sci U S A. 1975;72:1858–62. https://doi.org/10.1073/pnas.72.5.1858

Yao QQ, Wen J, Perrett S, Wu S. Distinct lipid membrane-mediated pathways of tau assembly revealed by single-molecule analysis. Nanoscale. 2022;14:4604–13. https://doi.org/10.1039/d1nr05960b

Ysselstein D, Joshi M, Mishra V, Griggs AM, Asiago JM, McCabe GP, et al. Effects of impaired membrane interactions on α-synuclein aggregation and neurotoxicity. Neurobiol Dis. 2015;79:150–63. https://doi.org/10.1016/j.nbd.2015.04.007

Zhaliazka K, Ali A, Kurouski D. Phospholipids and cholesterol determine molecular mechanisms of cytotoxicity of alpha-synuclein oligomers and fibrils. ACS Chem Neurosci. 2024;15:371–81. https://doi.org/10.1021/acschemneuro.3c00671

Zhang W, Falcon B, Murzin AG, Fan J, Crowther RA, Goedert M, et al. Heparin-induced tau filaments are polymorphic and differ from those in Alzheimer's and Pick's diseases. Elife. 2019;8: e43584. https://doi.org/10.7554/eLife.43584

SUPPORTING INFORMATION

Additional supporting information can be found online in the Supporting Information section at the end of this article.

How to cite this article: Ali A, Holman AP, Rodriguez A, Matveyenka M, Kurouski D. Tubulin-binding region alters tau–lipid interactions and changes toxicity of tau fibrils formed in the presence of phosphatidylserine lipids. Protein Science. 2024;33(7):e5078. https://doi.org/10.1002/pro.5078